CALPHAD: Computer Coupling of Phase Diagrams and Thermochemistry 43 (2013) 18–31

Contents lists available at ScienceDirect

CALPHAD: Computer Coupling of Phase Diagrams and Thermochemistry

journal homepage: www.elsevier.com/locate/calphad

CALPHAD description of the Mo–Re system focused on the sigma phase modeling ☆

R. Mathieu [a,*], N. Dupin [a], J.-C. Crivello [b], K. Yaqoob [b,1], A. Breidi [b,2], J.-M. Fiorani [c], N. David [c], J.-M. Joubert [b]

[a] Calcul Thermodynamique, 3 rue de l'avenir, 63670 Orcet, France
[b] Chimie Métallurgique des Terres Rares, Institut de Chimie et des Matériaux Paris-Est, CNRS, Université Paris-Est Créteil, 2-8 rue Henri Dunant, 94320 Thiais Cedex, France
[c] Institut Jean Lamour, Université de Lorraine, Vandoeuvre-les-Nancy 54506, France

ARTICLE INFO

Article history:
Received 27 June 2013
Received in revised form
31 July 2013
Accepted 5 August 2013
Available online 14 September 2013

Keywords:
Thermodynamic description
CALPHAD
Mo–Re
DFT-CEF
SQS
σ phase

ABSTRACT

The phase equilibria and thermodynamic properties of the Mo–Re system are studied by combining first-principle and CALPHAD approach. The mixing enthalpies in the bcc and hcp solution phases are estimated by first-principle calculations using the special quasirandom structures. The liquid, bcc and hcp phases are described by a substitutional solution model. The intermetallic phases, σ and χ, are described with the compound energy formalism with, respectively, 5 and 4 sublattices (SL) using the formation enthalpies of all the end-members directly from ab initio calculations. A phase diagram in agreement with the available experimental knowledge is obtained thanks to a least square procedure involving a limited number of parameters. Introducing all the elements in all the sublattices of the structure allows a proper description of the configuration of the intermetallic phases. Different simplifications of the description of the σ phase are considered. The ideal 4SL simplification is equivalent to the full description. The 3SL and 2SL models require excess parameters in order to fit reasonably the experimental phase diagram. Among these, only the $(Mo,Re)_{10}(Mo,Re)_{12}(Mo,Re)_8$ model allows to closely approximate the low temperature thermodynamic properties of the full description.

© 2013 The Authors. Published by Elsevier Ltd. All rights reserved.

1. Introduction

Ni based superalloys are commonly used for high temperature applications [1]. To enhance their properties, several alloying elements are used. Molybdenum and rhenium are among these. They can improve significantly the mechanical properties but present the drawback to form intermetallic compounds. Indeed, if their concentration is too large, topologically close packed (TCP) phases may form. These compounds constitute fragile sites for the initiation of rupture due to their brittleness and to their needle shape. Even when their formation does not initiate such dramatic damage, it weakens the matrix depleting strengthening elements [2]. The knowledge of their stability is thus of high technological interest.

The CALPHAD approach [3] allows to calculate phase equilibria in multicomponent alloys. However, up to now, it seems unable to describe accurately the stability of TCP phases [4]. This may be partially attributed to the limited experimental knowledge of these phases. It could be more deeply due to the complexity of these phases and to the oversimplification introduced by the thermodynamic models applied up to now.

The modeling of the σ phase with the compound energy formalism (CEF) was initially proposed by Andersson et al. [5] as $(A,B)_{16}(A)_4(B)_{10}$ based on the experimental knowledge of the site occupancies of some σ phases of interest for steels. As it was unable to describe the homogeneity range of some binary systems, Andersson and Sundman [6] proposed to modify it as $(A,B)_{18}(A)_4(B)_8$, losing most of the relation with the crystallographic structure. This second model has largely been used until Ansara et al. [7] recommended to come back to the 16/4/10 ratio, more crystallographically based. In the systems where the model $(A,B)_{16}(A)_4(B)_{10}$ was unable to describe the homogeneity of the σ phase, the introduction of *A* and *B* atom in the last sublattice (SL) was recommended, giving the $(A,B)_{16}(A)_4(A,B)_{10}$ model compatible with the initial one. Many systems have then been reassessed

☆This is an open-access article distributed under the terms of the Creative Commons Attribution-NonCommercial-No Derivative Works License, which permits non-commercial use, distribution, and reproduction in any medium, provided the original author and source are credited.

* Corresponding author. Tel.: +33 675771485.
E-mail address: rmathermo@free.fr (R. Mathieu).
[1] Present address: Department of Materials Engineering, School of Chemical and Materials Engineering (SCME), National University of Sciences and Technology, H-12, Islamabad, Pakistan.
[2] Present address: ICAMS/ STKS, Ruhr University Bochum, Universitatsstr. 90a, D-44789 Bochum, Germany.

0364-5916/$ - see front matter © 2013 The Authors. Published by Elsevier Ltd. All rights reserved.
http://dx.doi.org/10.1016/j.calphad.2013.08.002

and the new assessments have often considered both ratios 16/4/10 and 18/4/8 in order to handle the transition [8,9].

More recently, Joubert [10] produced an extensive analysis of the experimental site occupancies of the σ phase in many binary systems. He showed the different degrees of order achieved in the different systems as well as the peculiar behavior of the Cr and Re elements that can either play the role of *A* or *B* depending on the other element considered. He proposed a new model $(A,B)_{10}(A,B)_{20}$ allowing to easily change the role of *A* and *B* but neglecting the different occupancies often observed for the different highly coordinated sites. This proposition is highly appealing when assessing a description to develop a multicomponent database as it dramatically reduces the number of end-members to assess. However, it may be understood as going against the general tendency of improvement of the models with the higher performance of computational tools. While in the eighties, it was not reasonable to consider CEF with mixing in more than one sublattice, descriptions closer to the crystallography of the phase have become possible [11,12]. Moreover the assessment of the many end-members needed with models closer to the crystallography of the phase is made easier thanks to the increasing availability of results from first-principle (FP) calculations [10,13–18].

The improvements brought by the use of FP calculations are here studied in the particular case of the Mo–Re binary system. This study is part of a more extended project considering also other binary systems as well as a few ternary systems in order to determine the most suitable way to use FP results for real multicomponent systems. This first system presents the interest to have been described using different models up to now, allowing to compare the different models features.

In this paper, the information available on the system will first be briefly discussed. They consist of experimental data and first principles results as well as a summary of the different CALPHAD descriptions that will later be compared to our results. The different models used will then be presented and in particular the simplifications of the σ phase description. The results obtained with the complete description will then be compared to available experiments and other published assessments. Finally simplifications of the σ phase description will be discussed.

2. Bibliography

2.1. Experimental data

The experimental determination of the Mo–Re phase diagram was independently carried out by Dickinson and Richardson [19], Knapton [20] and Savitskii et al. [21,22] with the help of optical pyrometry, X-ray diffraction and metallographic methods. The alloys were mostly synthesized by arc-melting. Dickinson and Richardson [19] and Knapton [20] did not mention the purity of Mo and Re powders used for sample preparation, while the purity of powders employed by Savitskii et al. [21,22] was 99.8%.

All the authors identified five phases: liquid, molybdenum-rich bcc solid solution, σ phase, χ phase and rhenium-rich hcp solid solution. The crystal structure information of the stable phases is provided in Table 1. The σ crystal structure has a tetragonal unit cell commonly described with the space group $P4_2/mnm$, containing 30 atoms which occupy five different positions: 2*a*, 4*f*, $8i_1$, $8i_2$ and 8*j*. The site occupancies of the Mo–Re σ phase as a function of composition have been studied by [23–25]. A clear preference is observed for Mo, the larger atom, to occupy the high CN sites. The χ phase is isostructural with α-Mn and has a body centered cubic structure with 58 atoms per unit cell, that are distributed into four different crystallographical sites: 2*a*, 8*c*, $24g_1$ and $24g_2$. It belongs to the space group $I\bar{4}3m$. As for the σ phase, mixed occupancy is observed on all sites with a preference of Mo for high CN sites [25]. A detailed review of the crystal chemistry, homogeneity ranges and electron concentrations of σ and χ phases has been carried out by Joubert [10,26]. Some studies have reported an A15-type phase [27,28] in Mo–Re system, which is believed to be metastable. This phase may become stable at very low temperature [28] and does not appear in the phase diagram [29].

The σ phase was found to have wide homogeneity domain extending from 52 ± 2 at.% Re to 70 ± 2 at.% Re at 2673 K [29]. The σ phase is in particular formed as a primary phase from the liquid. Thanks to few sintered samples, Knapton proposed its eutectoid decomposition in bcc and χ phases. Even the most recent studies by Farzadfar et al. [25], Leonard et al. [30], Bei et al. [31] and Yaqoob and Joubert [32] have not resolved the uncertainty on this equilibrium. The χ phase is formed by a peritectoid reaction between the hcp and σ phases or by the eutectoid decomposition of the σ phase. The homogeneity domain of the χ phase is narrow ranging from 76 ± 1 to 79 ± 1 at.% Re at 2273 K [29].

Five invariant reactions in this system have been reported and are summarized in Table 2. The results reported by Savitskii et al. differ from those by Dickinson and Knapton about the phase relationship among liquid, bcc Mo and σ and invariant reactions. The experimental data of Knapton and Dickinson indicated that bcc Mo and σ phases form from liquid by a eutectic rather than a peritectic reaction. Thenceforward, the peritectic reaction of Savitskii et al. at 1773 K is to be considered as an eutectic. The different studies qualitatively agree upon the peritectic and peritectoid reactions. The temperatures of the first three invariants reported by [19–22] are quite different. This is somehow related to their very high values. In the open discussion reported at the end of Dickinson's paper [19], Knapton agreed that the temperatures reported by Dickinson [19] are probably more accurate than his temperatures, because of lower temperature gradient in the furnace used. The eutectoid reaction has only been evidenced by Knapton [20]. The σ phase is found to be stable at temperatures higher than 1423 K. By combining different experimental results, Knapton [20] concluded that the eutectoid reaction in the Mo–Re binary system takes place between 1373 K and 1423 K. As annealing temperatures in both [19] and [21,22] studies were higher than 1373 K, they were not able to detect the eutectoid decomposition of the σ phase into

Table 1
Crystallographic data of the σ, χ, bcc and hcp phases. CN: Coordination number; f_i: ratio of first neighbors in the same site.

Phase	Space group	Pearson symbol	Struktur-bericht	Proto-type	Wyckoff position (CN, f_i)
σ	$P4_2/mnm$	*tP*30	$D8_b$	CrFe	2*a* (12, 0), 4*f* (15, 0.07), $8i_1$ (14, 0.36), $8i_2$ (12, 0.08), 8*j* (14, 0.14)
χ	$I\bar{4}3m$	*cI*58	*A*12	α-Mn	2*a* (16, 0), 8 *c* (16, 0), $24g_1$ (13, 0.46), $24g_2$ (12, 0.25)
bcc	$Im\bar{3}m$	*cI*2	*A*2	W	2*a* (14, 1)
hcp	$P6_3/mmc$	*hPI*2	*A*3	Mg	2*c* (12, 1)

Table 2
Experimental and calculated invariant equilibria.

Invariant reaction	Type	T (K)	Re at.%			Reference
liquid+hcp ⇌ σ	Peritectic		liq	hcp	σ	
		2918	–	–	69	[19]
		2793	72	85	–	[20]
		2843	–	87	60	[21,22]
		2966	60	87	70	[8,45]
		2892	58	84	67	[25]
		2920	58	82	69	[46]
		2887	71	85.5	71.6	[47]
	Eutectic	2890	75	87.5	74	this work
liquid+σ ⇌ bcc	Peritectic		liq	bcc	σ	
		2773	–	–	49	[21,22]
liquid ⇌ σ+bcc	Eutectic		liq	bcc	σ	
		2778	49	42.5	53	[19]
		2713	50	43	–	[20]
		2745	46	41	54	[8,45]
		2799	45	43	54	[25]
		2786	44	42	53	[46]
		2777	44.2	40.8	50.2	[47]
		2737	38.3	38	53.1	this work
σ+hcp ⇌ χ	Perictectoid		σ	hcp	χ	
		2348	70	–	76	[19]
		2073–2123	–	91	–	[20]
		2123	67	91	78	[21,22]
		2225	70	89	78	[8,45]
		2343	70	89	77	[25]
		2269	70	92	77	[46]
		2129	69.3	91.3	77.4	[47]
		2186	69.3	88.4	76.7	this work
σ ⇌ bcc+χ	Eutectoid		σ	bcc	χ	
		1398	57	29	76	[20]
		1375	57	29	76	[8,45]
		1346	56	29	74	[25]
		1384	59	30	75	[46]
		1300	57.5	27.1	74.7	[47]
		1322	57.4	27.1	74	this work

bcc and χ phases. Farzadfar et al. [25] using similar experiments but longer heat treatments came to the same conclusions. However their high uncertainty is emphasized. The formation of the χ phase rather than the σ phase in sintered samples at lower temperature could be explained by kinetic reasons. The formation of the χ phase from a sample containing initially the σ phase formed at higher temperature has never been reported.

The Mo–Re phase diagram, proposed by Brewer and Lamoreaux [29], is based on the experimental data previously reported. The low temperature σ homogeneity range and the liquidus and solidus at Re more than 50 at.% are shown as dashed lines to express the uncertainty of the phase diagram in these fields.

2.2. First-principle calculations

Breidi et al. [33] have performed calculations of the mixing enthalpy in the bcc and hcp solution phases based on special quasirandom structure (SQS) [34] using the 32-atom [35] and 16-atom [36,37] SQS supercell models. An energy cutoff of 400 eV was used for the plane-wave basis set for calculations using SQS procedure. The SQS supercells were relaxed with respect to cell volume with spin polarized.

The mixing enthalpy in the phase φ is obtained from FP total energies by:

$$\Delta E^{\varphi}_{mix} = E^{\varphi}/n - \sum_i x_i E^{\varphi}_i \quad (1)$$

where E^{φ} is the FP total energy for n atoms, E^{φ}_i is the atomic total energy for the pure element i in the phase φ. However it happens very often, that one of these reference structures is dynamically unstable. The validity of the mixing energy derived is thus questionable. It can be interesting to rather express the formation energy of the composition under consideration:

$$\Delta E^{\varphi}_f = E^{\varphi}/n - \sum_i x_i E^{SER}_i \quad (2)$$

SER stands for the stable state for element i, *i.e.* bcc for Mo and hcp for Re. The instability of the reference state is then avoided but not the one of the disordered mixtures. This means that some of these results may not be reliable anyway. The mechanical instability is expected to occur somewhere between the two elements, hopefully close to the unstable structure. Results close to the stable element can be considered more reliable. The use of these energies within the CALPHAD approach is however not straightforward.

The formation energy for the pure element i in the phase φ is expressed as

$$\Delta E^{\varphi}_i = E^{\varphi}_i - E^{SER}_i \quad (3)$$

This values calculated from FP results at 0 K can be assimilated to the corresponding enthalpies. These are already described in the CALPHAD approach by the unary SGTE database [38,39]:

$$\Delta H^{\varphi}_i = H^{\varphi}_i - H^{SER}_i \quad (4)$$

Table 3
Structural energy or lattice stability values calculated by DFT: ΔE_i^{φ} [33] and by CALPHAD method: ΔH_i^{φ} [38,39].

i	φ	ΔE_i^{φ} (kJ/mol)	ΔH_i^{φ} (kJ/mol)
Mo	bcc	42.83	11.55
Re	hcp	30.58	17.00

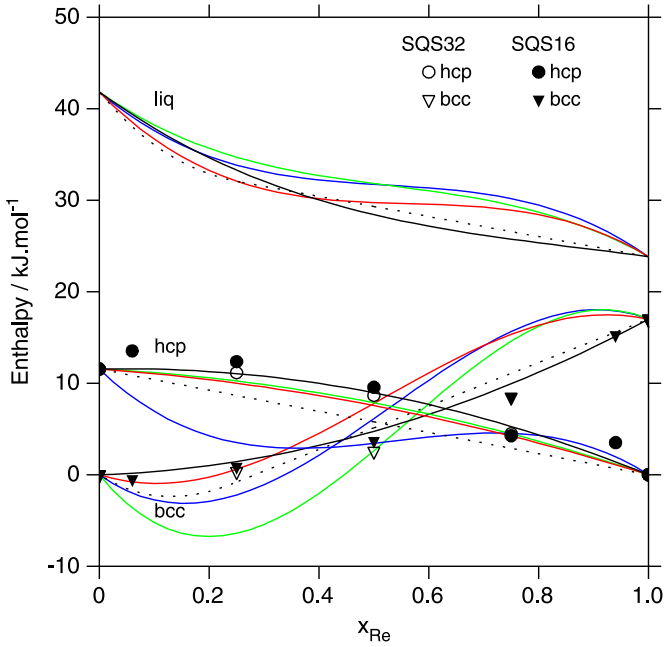


Fig. 1. The SQS enthalpies, calculated for 32 atoms and for 16 atoms [33], are compared to CALPHAD descriptions [8] in red, [25] in green, [45] in blue and [46] in black. Reference states are bcc Mo and hcp Re.

However the two sets of values are significantly different, as shown in Table 3, for Mo and Re of interest in the present work. This has already been noticed previously [40]. Kissavos et al. [41] have suggested that a rational method for coupling ab initio and CALPHAD techniques might be the utilization of ab initio results while retaining the CALPHAD lattice stabilities in the calculation of phase diagrams. In order to use the SQS values in the CALPHAD procedure, the mixing energies from DFT can be directly used as mixing enthalpies however the formation energies must be rescaled. The formation enthalpies are thus expressed as follows:

$$\Delta H_f^{\varphi} = \Delta E_{mix}^{\varphi} + x_{\mathrm{Mo}} \Delta H_{\mathrm{Mo}}^{\varphi} + x_{\mathrm{Re}}\ \Delta H_{\mathrm{Re}}^{\varphi} \tag{5}$$

The formation enthalpies calculated from Eq. (5) are shown as symbols in Fig. 1. The results calculated by the different SQS methods are very close. They show a rather regular behavior of the mixing enthalpy for both phases. This figure shows repulsive interaction in the hcp solid solution with a mixing enthalpy between 0 and 3 kJ/mol, indicating that a metastable miscibility gap would exist at low temperatures. For the bcc solid solution, attractive interactions are found with a mixing enthalpy between −6 and 0 kJ/mol, indicating a tendency for intermixing between Mo and Re in the bcc structure.

Crivello et al. [14,17,42] and Palumbo et al. [18] have performed Density Functional Theory (DFT) calculations [43,44] for the 32 σ and 16 χ ordered configurations generated by the complete occupancy of each site by one or the other element. For every configuration, DFT calculations have been done in the same conditions and convergence criteria, using the Vienna ab initio simulation package (VASP). Total energy results obtained by Crivello et al. [42] are listed in Tables 4 and 5. The corresponding mixing and formation values calculated with equations similar to Eqs. (1) and (2) are also presented. The mixing enthalpies are rather named ordering enthalpies as the mixing is accompanied by ordering for these phases. The formation enthalpy of all the calculated configurations is shown in Fig. 2 as open symbols.

2.3. Available descriptions in Mo–Re system

Thermodynamic assessments of the Mo–Re binary system have previously been published by Mao et al. [8] with corrigendum [45], Farzadfar et al. [25] and Yang et al. [46]. The calculated Mo–Re phase diagrams show, in general, a good agreement with the experimental information. The main differences lie in the thermodynamic models used to describe the σ and χ phases as summarized in Table 6. Mao et al. [8,45] have used the two classical models [5,7] for the σ phase, but only the $(Mo,Re)_{18}(Mo)_4(Re)_8$ model is discussed in the present study as the reported description for the other one does not allow to reproduce the published figures. Farzadfar et al. [25] applied the 2SL model proposed by Joubert [10]. This work is characterized by the fit of the experimental site occupancies of the intermetallic phases. Yang et al. [46] applied a model considering the mixing on two sublattices with a limited composition range from Mo_2Re to Re using DFT calculations in order to better assess the end-members.

In these thermodynamic assessments [8,25,45,46], the authors have used excess parameters which denote interactions between constituents in a sublattice. Mao et al. [8,45] have introduced only one constant parameter for σ phase and none for χ phase. Farzadfar et al. [25] have introduced one function of temperature for σ phase and a constant one for χ phase. Yang et al. [46] have introduced two excess parameters for σ phase and one for χ phase. These values are either negative or positive, *i.e.* increase or decrease the mixing given by the Gibbs energies of formation of the stoichiometric compounds.

A new description of the system using models for the σ and χ phase in which all the elements are considered in all the sublattices defined by their crystallographic structure has been proposed by Dupin et al. [47]. Besides available experimental information, the same DFT for the σ and χ phases [14,17,42] used in the present work has been taken into account. This thermodynamic description shows a good agreement with experimental data without excess Gibbs energy terms for the σ and χ phases. The simplification of the σ model was also investigated. The need to introduce interaction parameters was shown in order to keep reasonable agreement with experiments when using 3SL or 2SL model. The present work thus mainly differs from this one by the use of SQS for the solutions phases.

3. Thermodynamic modeling

The CALPHAD approach requires the modeling of the Gibbs energy of each phase constituting the system under consideration. The equations used in the present work are presented hereunder.

3.1. Solution phases

Liquid, hcp and bcc phases are described as substitutional solutions. The Gibbs energy for a given phase φ is described as a function of its atomic composition (x_{Mo}, x_{Re}) as the sum:

$$G^{\varphi} = G^{ref,\varphi} + G^{id,\varphi} + G^{xs,\varphi} + G^{phys,\varphi} \tag{6}$$

where

$$G^{ref,\varphi} = x_{\mathrm{Mo}} G_{\mathrm{Mo}}^{\varphi} + x_{\mathrm{Re}} G_{\mathrm{Re}}^{\varphi} \tag{7}$$

Table 4
First-principle enthalpies of σ phase at 0 K. The end-members used in each simplification named after Table 7 are indicated by shaded boxes. E^{σ} correspond to the DFT total energies, calculated for 30 atoms from [42]. ΔH_f, resp. ΔH_{ord}, correspond to these energies referred to bcc Mo and hp Re, resp. to the σ phase of the pure elements.

Occupancy					Re	E^{σ}	ΔH_f	ΔH_{ord}	4SL	3SL-35	3SL-23	3SL-25	2SL
2a	4f	$8i_1$	$8i_2$	8j	at.%	(eV)	(kJ/mol)	(kJ/mol)		×	+	●	
Mo	Mo	Mo	Mo	Mo	0	−323.48	16.10	0.00					
Re	Mo	Mo	Mo	Mo	7	−327.23	13.51	−2.14					
Mo	Re	Mo	Mo	Mo	13	−329.39	16.05	0.85					
Re	Re	Mo	Mo	Mo	20	−332.95	14.05	−0.69					
Mo	Mo	Re	Mo	Mo	27	−336.27	12.85	−1.45					
Mo	Mo	Mo	Re	Mo	27	−338.81	4.69	−9.61					
Mo	Mo	Mo	Mo	Re	27	−336.42	12.37	−1.92					
Re	Mo	Re	Mo	Mo	33	−340.10	10.00	−3.84					
Re	Mo	Mo	Re	Mo	33	−342.64	1.83	−12.01					
Re	Mo	Mo	Mo	Re	33	−340.04	10.20	−3.64					
Mo	Re	Re	Mo	Mo	40	−342.25	12.57	−0.82					
Mo	Re	Mo	Re	Mo	40	−344.38	5.72	−7.67					
Mo	Re	Mo	Mo	Re	40	−341.90	13.70	0.31					
Re	Re	Re	Mo	Mo	47	−345.81	10.60	−2.34					
Re	Re	Mo	Re	Mo	47	−347.97	3.65	−9.29					
Re	Re	Mo	Mo	Re	47	−345.25	12.42	−0.52					
Mo	Mo	Re	Re	Mo	53	−350.88	3.78	−8.71					
Mo	Mo	Re	Mo	Re	53	−348.27	12.15	−0.34					
Mo	Mo	Mo	Re	Re	53	−350.94	3.57	−8.91					
Re	Mo	Re	Re	Mo	60	−354.69	0.99	−11.05					
Re	Mo	Re	Mo	Re	60	−351.79	10.31	−1.73					
Re	Mo	Mo	Re	Re	60	−354.49	1.62	−10.42					
Mo	Re	Re	Re	Mo	67	−356.31	5.26	−6.33					
Mo	Re	Re	Mo	Re	67	−353.54	14.15	2.57					
Mo	Re	Mo	Re	Re	67	−355.89	6.60	−4.99					
Re	Re	Re	Re	Mo	73	−359.89	3.23	−7.91					
Re	Re	Re	Mo	Re	73	−356.82	13.08	1.95					
Re	Re	Mo	Re	Re	73	−359.22	5.37	−5.77					
Mo	Mo	Re	Re	Re	80	−361.71	6.85	−3.83					
Re	Mo	Re	Re	Re	87	−365.12	5.34	−4.89					
Mo	Re	Re	Re	Re	93	−366.48	10.46	0.68					
Re	Re	Re	Re	Re	100	−369.77	9.33	0.00					

Table 5
First-principle enthalpies of χ phase at 0 K. E^{χ} correspond to the DFT total energies, calculated for 58 atoms from [42]. ΔH_f, resp. ΔH_{ord}, correspond to these energies referred to bcc Mo and hp Re, resp. to the χ phase of the pure elements.

Occupancy				Re at.%	E^{χ} (eV)	ΔH_f (kJ/mol)	ΔH_{ord} (kJ/mol)
2a	8c	$24g_1$	$24g_2$				
Mo	Mo	Mo	Mo	0	−619.36	26.13	0.00
Re	Mo	Mo	Mo	3	−621.99	26.65	1.26
Mo	Re	Mo	Mo	14	−630.44	27.31	4.11
Re	Re	Mo	Mo	17	−632.90	28.11	5.64
Mo	Mo	Re	Mo	41	−662.01	13.98	−3.36
Mo	Mo	Mo	Re	41	−667.06	5.59	−11.75
Re	Mo	Re	Mo	48	−664.70	19.32	3.44
Re	Mo	Mo	Re	48	−669.43	11.45	−4.43
Mo	Re	Re	Mo	55	−672.07	16.86	2.44
Mo	Re	Mo	Re	55	−676.65	9.24	−5.18
Re	Re	Re	Mo	59	−674.44	17.81	4.13
Re	Re	Mo	Re	59	−678.64	10.84	−2.85
Mo	Mo	Re	Re	83	−706.53	−1.26	−9.82
Re	Mo	Re	Re	86	−708.86	−0.24	−8.07
Mo	Re	Re	Re	97	−715.48	3.46	−2.17
Re	Re	Re	Re	100	−717.56	4.90	0.00

$$G^{id,\varphi} = RT(x_{Mo}\ln x_{Mo} + x_{Re}\ln x_{Re}) \tag{8}$$

$$G^{xs,\varphi} = x_{Mo}x_{Re}\sum_{\nu=0}^{n} L^{\varphi,\nu}_{Mo,Re}(x_{Mo}-x_{Re})^{\nu} \tag{9}$$

The description for the pure components in the different phases, G^{φ}_{Mo} and G^{φ}_{Re}, is taken from the SGTE unary database [38,39]. The $G^{phys,\varphi}$ stands for the magnetic contribution [39], and is obviously not considered in the present work. The ideal contribution $G^{id,\varphi}$ expresses the random mixing of the different elements constituting the phase. The excess contribution $G^{xs,\varphi}$ corresponds to the interaction between the elements in the phase. It is described by a Redlich–Kister polynomial [48], where the binary interaction parameters, $L^{\varphi,\nu}_{Mo,Re}$, are expressed as linear functions of temperature. The few experimental phase diagram data being quite inaccurate, the different variables expressing the liquid excess are not much constrained. It is thus introduced relationship between the liquid and bcc parameters.

3.2. Intermetallic compounds

3.2.1. σ phase full description

Ideally, a thermodynamic model of the σ phase should consider its five different sites. In the present work, the Mo–Re σ phase is described by using the 5SL CEF [11,49]:

$$(Mo,Re)_2(Mo,Re)_4(Mo,Re)_8(Mo,Re)_8(Mo,Re)_8.$$

Its Gibbs energy is thus expressed as

$$G^{\sigma} = \sum_{ABCDE} y_A^{2a} y_B^{4f} y_C^{8i_1} y_D^{8i_2} y_E^{8j} G^{\sigma}_{ABCDE} + RT\sum_s a^s \sum_i y_i^s \ln y_i^s \tag{10}$$

where

$$G^{\sigma}_{ABCDE} - \sum_s a^s G_i^{SER} = E^{\sigma}_{ABCDE} - \sum_s a^s E_i^{SER} - T\sum_s a^s\, \Delta S_i^{\sigma} \tag{11}$$

where y_i^s is the site fraction of component i in sublattice s, G^{σ}_{ABCDE} is the Gibbs free energy of the end-member $ABCDE$, R is the gas

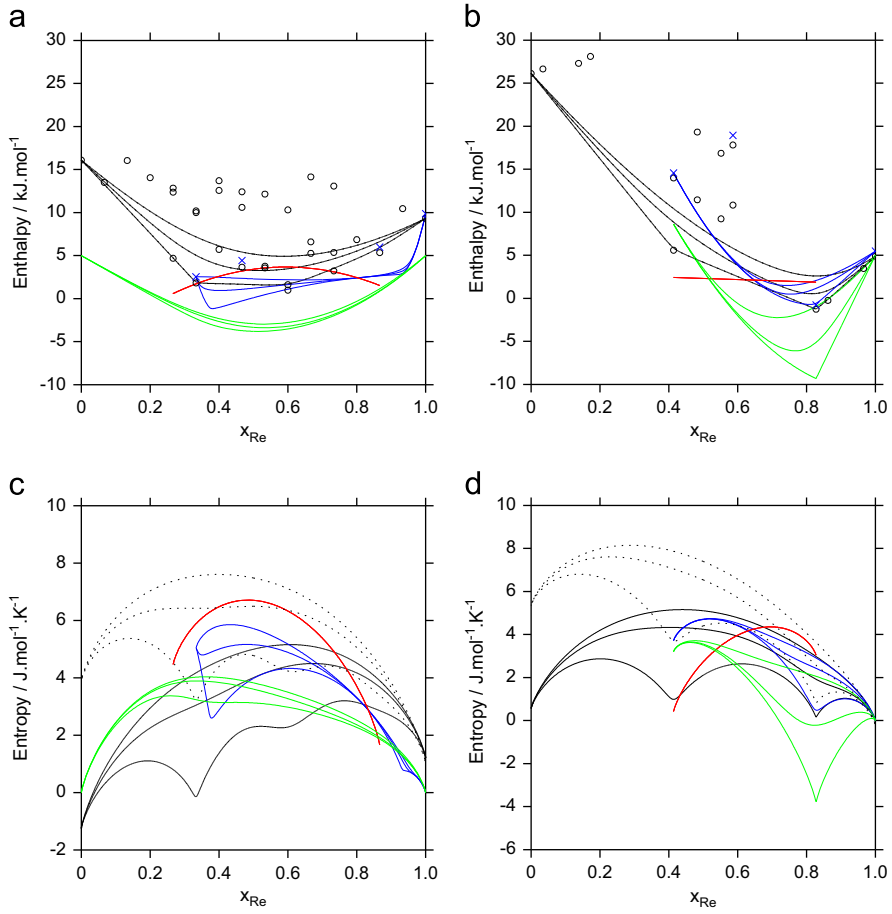


Fig. 2. Enthalpies and entropies of formation of the σ phase (a, c) and χ phase (b, d). The open symbols correspond to the DFT results presented in Tables 4 and 5. The blue crosses correspond to the DFT results from Yang et al. [46]. The different sets of line, calculated at 500, 1500 and 2500 K, correspond to different descriptions: in red from Mao et al. [8,45], in green from Farzadfar et al. [25], in blue from Yang et al. [46], as dotted black line from Dupin et al. [47] and in black from the present study. Reference states are bcc Mo and hcp Re at the current temperature. (For interpretation of the references to color in this figure caption, the reader is referred to the web version of this paper.)

Table 6
Thermodynamic models for σ and χ phases used in previous Mo–Re assessments [8,25,45–47].

σ phase	χ phase	Ref.
1: $(Mo,Re)_{16}(Mo)_4(Re)_{10}$ 2: $(Mo,Re)_{18}(Mo)_4(Re)_8$	$(Mo)_{10}(Re)_{24}(Mo,Re)_{24}$	[8,45]
$(Mo,Re)_{10}(Mo,Re)_{20}$	$(Mo,Re)_{10}(Mo,Re)_{24}(Re)_{24}$	[25]
$(Mo,Re)_{16}(Mo,Re)_4(Re)_{10}$	$(Mo,Re)_{10}(Mo,Re)_{24}(Re)_{24}$	[46]
$(Mo,Re)_2(Mo,Re)_4(Mo,Re)_8$ $(Mo,Re)_8(Mo,Re)_8$	$(Mo,Re)_2(Mo,Re)_8(Mo,Re)_{24}(Mo,Re)_{24}$	[47]

Table 7
Descriptions of the simplified models.

Name	Model	Assumption	Number of compounds
5SL	$(Mo,Re)_2(Mo,Re)_4$ $(Mo,Re)_8(Mo,Re)_8(Mo,Re)_8$	G^{5SL}_{ABCDE}	32
4SL	$(Mo,Re)_{10}(Mo,Re)_4$ $(Mo,Re)_8(Mo,Re)_8$	$G^{4SL}_{ABCD} = G^{5SL}_{ABCAD}$	16
3SL-35	$(Mo,Re)_{10}(Mo,Re)_4(Mo,Re)_{16}$	$G^{3SL}_{ABC} = G^{5SL}_{ABCAC}$	8
3SL-23	$(Mo,Re)_{10}(Mo,Re)_{12}(Mo,Re)_8$	$G^{3SL}_{ABC} = G^{5SL}_{ABBAC}$	8
3SL-25	$(Mo,Re)_{10}(Mo,Re)_{12}(Mo,Re)_8$	$G^{3SL}_{ABC} = G^{5SL}_{ABCAB}$	8
2SL	$(Mo,Re)_{10}(Mo,Re)_{20}$	$G^{2SL}_{AB} = G^{5SL}_{ABBAB}$	4

constant, a^s is the number of sites of sublattice s, E^{σ}_{ABCDE} and E^{SER}_i are the DFT energy of the compound *ABCDE* in the σ structure and of the element i in its stable structure respectively. G^{SER}_i is the Gibbs energy of the element i in its SER state, as described from SGTE database [38]. ΔS^{σ}_i is the difference entropy of the element i between its σ structure and its stable structure *i.e.* $S^{\sigma}_i - S^{SER}_i$. The sum over s in Eq. (11) is expressed considering the element i in the sublattice s defined by the compound *ABCDE*, *i.e.* i in the first sublattice is *A*, i in the second sublattice is *B*… During the present study, it is assumed that all the interactions characterizing the phase are taken into account by the DFT calculations and thus, no excess terms are used for the σ phase. The only parameters assessed during the present study for this phase are the two ΔS^{σ}_i terms.

3.2.2. σ phase simplification

Within the 5SL-CEF, the number of end-members to be considered significantly increases in multicomponent systems: 32 in a binary system, 243 in a ternary system and 1024 in a quaternary system. Some simplifications can be adopted in order to reduce the number of sublattices.

By coupling Wyckoff positions of the same or similar coordination number and close experimental site occupancy, a four-sublattice model (4SL), three different three-sublattice models (3SL-35, 3SL-23, 3SL-25) and a two-sublattice model (2SL) have been defined for the σ phase as summarized in Table 7. The end-members used in the 4SL simplification have the same element in the 2*a* and 8*i*2 sites. This assumption is based on the similar experimental occupancies

reported for these sites in most σ phases. End-members used in the 3SL and 2SL simplifications also fulfill this requirement. The 3SL-35 model takes into account the compounds that have the same element in the $8i_1$ and $8j$, both of CN14. 3SL-35 means 3SL grouping sites 1+4 and 3+5. This corresponds to the classical simplification [5,7], but where all the elements are considered in all sublattices. When sites $4f$ and $8i_1$ are merged into one sublattice, the 3SL-23 model is obtained. 3SL-23 means 3SL grouping sites 1+4 and 2+3. When sites $4f$ and $8j$ are merged, the 3SL-25 model is yielded. 3SL-25 means 3SL grouping sites 1+4 and 2+5. Finally, the three sites with the higher coordination numbers: $4f$, $8i_1$ and $8j$ may be grouped which gives the model $(A,B)_{10}(A,B)_{20}$ as proposed by Joubert [10]. In all these models, all the elements are considered in all sublattices. The end-members actually used for each of these simplifications are shown as dashed box in Table 4.

The following equations for the Gibbs free energy are used for each of these models:

$$G^{\sigma-4SL} = \sum_{ABCE} y_A^{2a+8i_2} y_B^{4f} y_C^{8i_1} y_E^{8j} G^{\sigma}_{ABCE} + RT\sum_s a^s \sum_i y_i^s \ln y_i^s + G^{\sigma-4SL,ex} \quad (12)$$

$$G^{\sigma-3SL-35} = \sum_{ABC} y_A^{2a+8i_2} y_B^{4f} y_C^{8i_1+8j} G^{\sigma}_{ABC} + RT\sum_s a^s \sum_i y_i^s \ln y_i^s + G^{\sigma-3SL-35,ex} \quad (13)$$

$$G^{\sigma-3SL-23} = \sum_{ABC} y_A^{2a+8i_2} y_B^{4f+8i_1} y_C^{8j} G^{\sigma}_{ABC} + RT\sum_s a^s \sum_i y_i^s \ln y_i^s + G^{\sigma-3SL-23,ex} \quad (14)$$

$$G^{\sigma-3SL-25} = \sum_{ABC} y_A^{2a+8i_2} y_B^{4f+8j} y_C^{8i_1} G^{\sigma}_{ABC} + RT\sum_s a^s \sum_i y_i^s \ln y_i^s + G^{\sigma-3SL-25,ex} \quad (15)$$

$$G^{\sigma-2SL} = \sum_{AB} y_A^{2a+8i_2} y_B^{CN} + G^{\sigma}_{AB} + RT\sum_s a^s \sum_i y_i^s \ln y_i^s + G^{\sigma-2SL,ex} \quad (16)$$

The first two terms appearing in Eqs. (12)–(16) correspond to the reference and ideal terms. As some of the configurations of the full 5SL description are ignored, excess contribution is added in order to describe the missing interactions. They are expressed in the form, $G^{\sigma spl,ex} = y^s_{Mo} y^s_{Re} L^{\sigma spl,s}_{Mo,Re}$, where the s sublattice corresponds to the one obtained merging different sites.

3.2.3. χ phase

In this study, the χ phase is modeled as $(Mo,Re)_2(Mo,Re)_8(Mo,Re)_{24}(Mo,Re)_{24}$, using a 4SL-CEF. As for the σ phase, the FP calculated energies of formation at 0 K for the end-members of the χ phase (Table 5) are directly used as enthalpies of formation in the CEF, no excess terms are considered. The two ΔS^{χ}_i are assessed from phase diagram information.

3.3. Optimization procedure

The parameters of the thermodynamic model presented above, $L^{liq}_{Mo,Re}$, $L^{bcc}_{Mo,Re}$, $L^{hcp}_{Mo,Re}$, ΔS^{σ}_{Mo}, ΔS^{σ}_{Re}, ΔS^{χ}_{Mo} and ΔS^{χ}_{Re}, have been assessed following a computer-assisted statistical procedure [3] using the PARROT module [50] of the Thermo-Calc software [51] in order to obtain the best fit to the experimental and SQS data first using the 5SL DFT-CEF for the σ phase.

Then, the excess interaction parameters for the different simplifications of the σ phase description have been assessed keeping unchanged the description of the other phases (χ, liquid, bcc, hcp) and the values of ΔS^{σ}_i previously assessed with the full σ description. The interaction parameters assessed using the same pop file [50], *i.e.* the same experimental information as with the full description, allow to keep almost unchanged the calculated phase diagram.

The assessed parameters are presented in Table 8.

Table 8
List of optimized parameters (J mol^{-1}).

	Parameter
Phase	
liquid	$L^{liq,0}_{Mo,Re} = L^{bcc,0}_{Mo,Re} - 2610$
	$L^{liq,1}_{Mo,Re} = L^{bcc,1}_{Mo,Re} - 7790$
bcc	$L^{bcc,0}_{Mo,Re} = -15,025 + 11.404T$
	$L^{bcc,1}_{Mo,Re} = 8.07T$
hcp	$L^{hcp,0}_{Mo,Re} = 12,740 + 1.951T$
σ	$\Delta S^{\sigma}_{Mo} = -1.251$
	$\Delta S^{\sigma}_{Re} = 1.205$
χ	$\Delta S^{\chi}_{Mo} = 0.5596$
	$\Delta S^{\chi}_{Re} = -0.0905$
σ/Model	
3SL-23	$L^0_{*:Mo,Re:*} = -48,000 + 7.79T$
3SL-25	$L^0_{*:Mo,Re:*} = -67,750 + 2.71T$
3SL-35	$L^0_{*:*:Mo,Re} = -130,000 - 1.1T$
2SL	$L^0_{*:Mo,Re} = -242,810 + 11.4T$

4. Results and discussions

4.1. Description with the full 5SL-CEF for the σ phase

4.1.1. Thermodynamic properties

Fig. 1 compares the enthalpy curves from our CALPHAD descriptions with the SQS results. This description optimized using the SQS32 results is as well in satisfactory agreement with the SQS16. The bcc curve, however, does not capture exactly the asymmetry of the values predicted by first-principles. When the mixing curve better fits them, agreement with the phase diagram data becomes much less satisfactory. During the optimization procedure, experimental phase diagram and SQS data were weighted in order to get a compromise.

The calculated curves from previous studies are also plotted for comparison. All the CALPHAD descriptions agree well with the hcp SQS on the Re rich side. This is due to the fact that this part of the curve is very much constrained by phase diagram data. However, Yang et al. [46] largely deviate when decreasing the Re content where the phase is not stable. This can be explained by the fact that they are using a subregular excess contribution allowing more freedom than can be fitted from the only phase diagram information.

For the bcc phase, the situation is quite different. Our curve is the closer to the SQS values. This is to be expected as these values are used during the present work. Even if Dupin et al. [47] description did not use the SQS results, it is actually also rather close but significantly more negative in the Mo-rich area. The other descriptions show a mixing enthalpy less regular than predicted by SQS. The asymmetry of these descriptions is thus not characteristic of the interaction of Mo and Re in this phase but an artefact coming from overfitting of the bcc thermodynamic behavior on the σ solvus, possibly counterbalancing the weakness of the σ description. However Yang et al. [46] and Mao et al. [8,45] descriptions, also without using SQS results, stay in reasonable agreement on the Mo rich side where the phase is stable. Farzadfar [25] significantly overestimates the mixing enthalpy in the Mo rich side.

The liquid mixing enthalpy calculated with the different descriptions is surprisingly close. There is no information on this behavior, either experimental or theoretical, to compare with these calculations. As for the bcc phase, our description shows the most regular behavior.

Fig. 2 shows the enthalpy and entropy of the σ and χ phases calculated at 500, 1500 and 2500 K with the present description.

They are compared to DFT values shown as open circles. At low temperature, the enthalpy is close to the most stable DFT energies. At higher temperature, the expansion provided by the CEF yields smoother enthalpy curves. Temperature decreases the degree of order, increases the configurational entropy and decreases the absolute ordering enthalpy.

The behavior calculated from previous descriptions are also plotted for comparison. Dupin et al. [47] enthalpy curves are identical to the present ones as the same DFT energies were used. However, the entropy curves are different as the ΔS_i^{σ} are different due to the use of SQS for the solution phases in our study. Higher ΔS_{Mo}^{σ} were obtained in order to stabilize the σ phase with respect to the bcc phase that had a slightly more negative mixing enthalpy. This difference is actually quite high, about 5 kJ/mol/K for both phases. An estimation of this value by FP approach would be of high interest in order to be sure that this difference is not related to the fact that the information currently available on the system which do not allow to totally constrain the description.

The other descriptions [8,45,25,46] show significant differences with DFT information. Indeed, enthalpies from Fardzafar et al. [25] are significantly more stabilizing than DFT data for the two phases. For the σ phase, this can be related to the assumption taken for the pure elements. The 5 kJ/mol used is significantly lower than the DFT values. The formation of the χ phase of ideal stoichiometry Mo_5Re_{24} is about 10 kJ/mol, more exothermic than predicted by DFT at low temperature. This is compensated by too low entropy in the range of stability of the phase. In the description of Mao [8,45], the mixing occurs on only one site and so no constitutional disorder is possible. Thus, enthalpy and entropy do not vary with temperature. The entropy was only modeled as formation entropy of the end-members. Underestimating the configurational entropy is an important cause of bad extrapolation in multicomponent systems. For Yang et al. [46], the mixing occurs on two sites and so a constitutional disorder is possible. This description was fitted using DFT results for some compounds, shown as blue crosses in Fig. 2. Nevertheless, due to a limited range of composition with an end-member close to the σ stability range, the separation between vibrational and configurational entropy was neither properly described. This description defines a high entropy for the stoichiometric end-point MoReReMoRe, in order to fit the phase diagram while the full 5SL description shows that the configurational entropy changes dramatically with temperature at this composition. This problem does not appear in the case of the χ as the end-point ReReMoRe is rather far from the composition where the phase is stable. The change of the configurational entropy in the χ homogeneity range is then very close to the 4SL description.

The site occupancies of Re calculated at 500, 1500 and 2500 K are shown in Fig. 3 for the σ phase and Fig. 4 for the χ phase. For both phases, the occupancy sequence clearly indicates that Re has a preference for lower CN sites. In the σ phase, Re first occupies only the CN12 sites, 2*a* and 8i_2, with close site occupancies. Increasing the Re content, Re replaces Mo on the two CN14 sites, 8i_1 and 8*j*, also with close site fractions. At 500 K, it is first the 8i_1 that is occupied, and later the 8*j*. However the very small difference in energy of the compounds ReMoReReMo and ReMoMoReRe yields to a similar behavior of these sites when temperature increases. Finally, at high

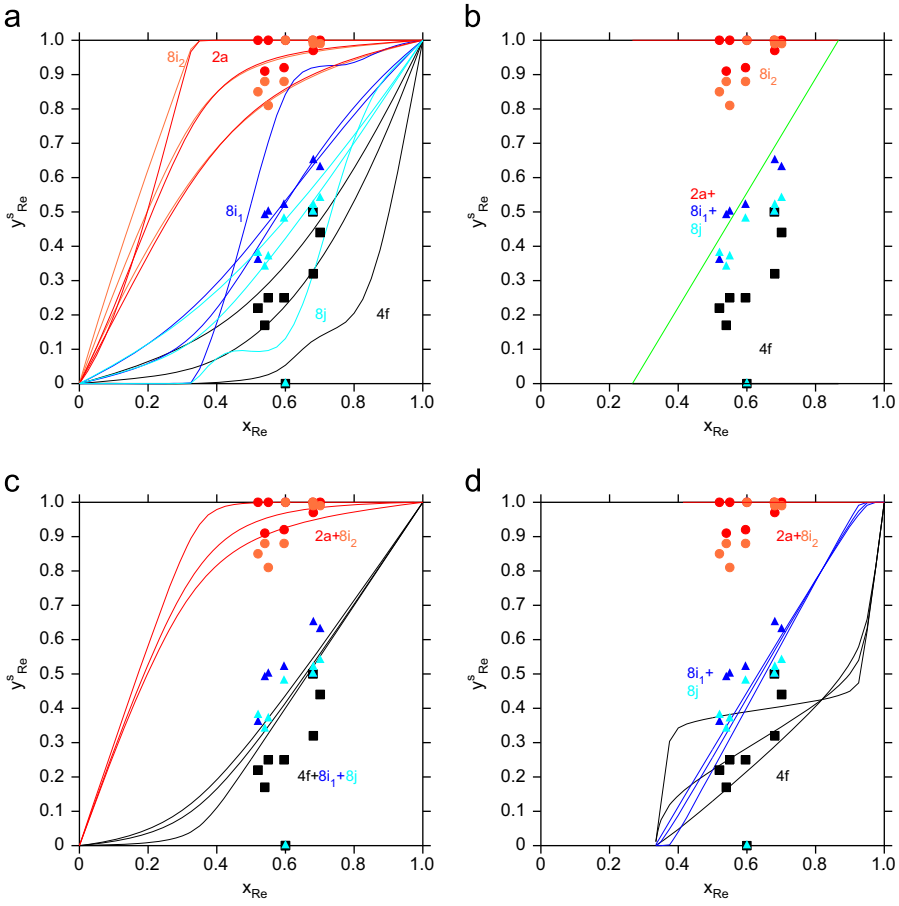


Fig. 3. Comparison of σ experimental site occupancies determined by [25,23,24] on samples heat treated at 1473 and 1873 K with calculated ones at 500, 1500 and 2500 K using the description from (a) this study, (b) Mao et al. [8,45], (c) Farzadfar et al. [25] and (d) Yang et al. [46].

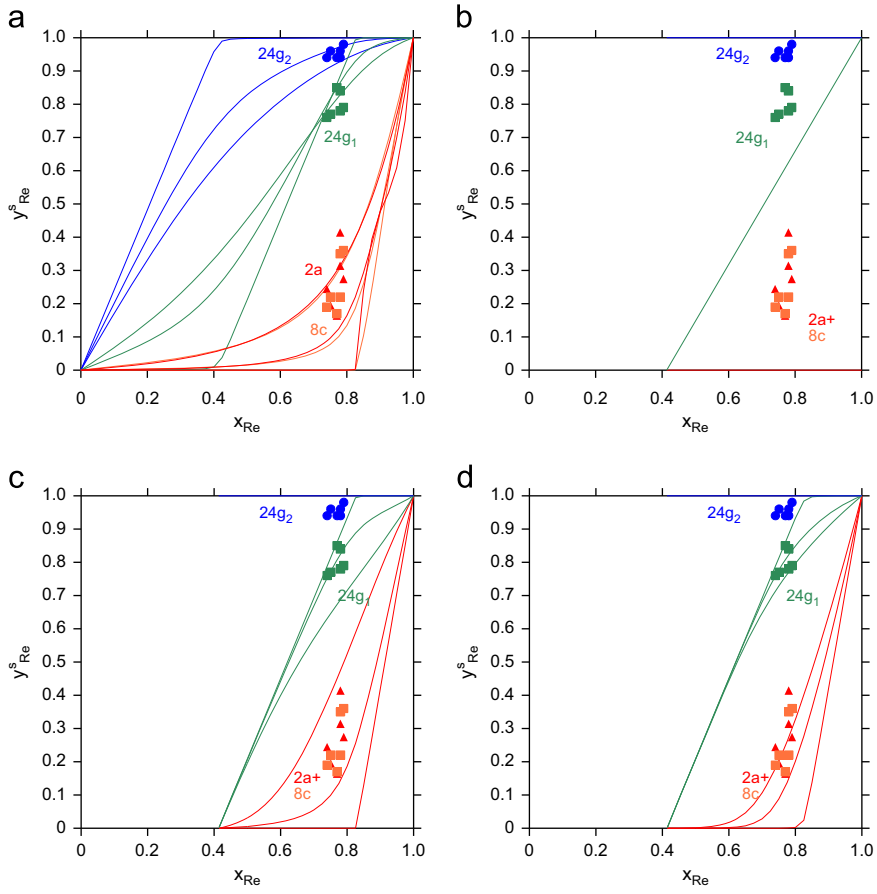


Fig. 4. Comparison of χ experimental site occupancies determined by [25,23,24] on samples heat treated at 1473, 1873 and 2273 K with calculated ones at 500, 1500 and 2500 K using the description from (a) this study, (b) Mao et al. [8,45], (c) Farzadfar et al. [25] and (d) Yang et al. [46].

Re concentration, Re replaces Mo on the CN15 site (4*f*). The decrease of order with temperature is shown by the fact that the different curves are approaching the diagonal corresponding to disorder. However a clear separation of the different sites remains: CN12 on one side, CN14 and CN15 on the other one. A comparable behavior is found for the χ phase. First, Mo is replaced by Re on the CN12 site ($24g_2$), then on the CN13 site ($24g_1$) and finally, simultaneously on the CN16 sites (2*a* and 8*c*). Whatever the temperature, the general sequence is similar. At 1473 K, 1873 K and 2273 K, experimental site occupancies are available [24,25]. They compare well with the computed values. This agreement validates the use of DFT to describe the ordering in the σ and χ phases with respectively the 5SL-CEF and 4SL-CEF.

In Figs. 3 and 4, the calculated site occupancies from previous studies are also plotted for comparison. The model proposed by Dupin et al. being very close to the one from this study, the site occupancies are equivalent, and so not discussed. Mao et al. simplified the σ phase by combining 2*a*, $8i_1$ and 8*j* together allowing mixing keeping $8i_2$ only occupied by Re and 4*f* only by Mo. Only the $8i_1$ and 8*j* site fractions agree well with experiments (Fig. 3b). Reasonable agreement is found for the descriptions from Farzadfar et al. (Fig. 3c) and from Yang et al. (Fig. 3d).

For the χ phase, Mao et al. (Fig. 4b) have simplified by allowing only Mo in 2*a* and 8*c*, only Re in $24g_2$ and mixing on $24g_1$. As for the σ phase, the agreement is rather poor. Fardzafar et al. (Fig. 4c) and Yang et al. (Fig. 4d) have simplified the model combining the 2*a* and 8*c* and excluding Mo from $24g_2$. The calculated site fraction of Mo for this sublattice is thus zero for any composition. A reasonable agreement between calculation and experiment is reached for the site fractions on the different sublattices.

However, the description of Mao et al. is not able to describe the different occupancies observed experimentally on the site of 4*f* for σ phase and $2a+8c$ for χ phase because it assumes complete occupancy of these sites by Mo. The fact that either Yang or our description is using FP results does not improve dramatically the agreement with experimental site occupancies with respect to Farzadfar et al. This is somehow related to the fact that the experimental site occupancies were used by Farzadfar et al. in their optimization procedure. This procedure however did not allow to separate properly the entropy and enthalpy contribution as discussed from Fig. 2.

Our description is the closer to experimental information. It is of course possible thanks to the use of a model taking into account all the complexity of crystallographic structure under consideration. It is interesting that its agreement comes directly from DFT calculations and not from a fitting procedure like in Farzadfar's work. It allows to validate first of all the accuracy of DFT results and second the use of the CEF in order to expand these in temperature.

4.1.2. *Phase diagrams*

The phase diagram calculated after the present parameter optimization is compared with the experimental data from Dickinson and Richardson [19], Knapton [20], Savitskii et al. [21,22], Farzadfar et al. [25] and Yaqoob and Joubert [32] works in Fig. 5. Discrepancies are noticeable in three regions: the homogeneity range for σ phase at low temperature, the hcp solvus at low temperatures and finally the melting temperatures. They are the regions where a large uncertainty remains on the experimental knowledge. For the low temperatures, the time

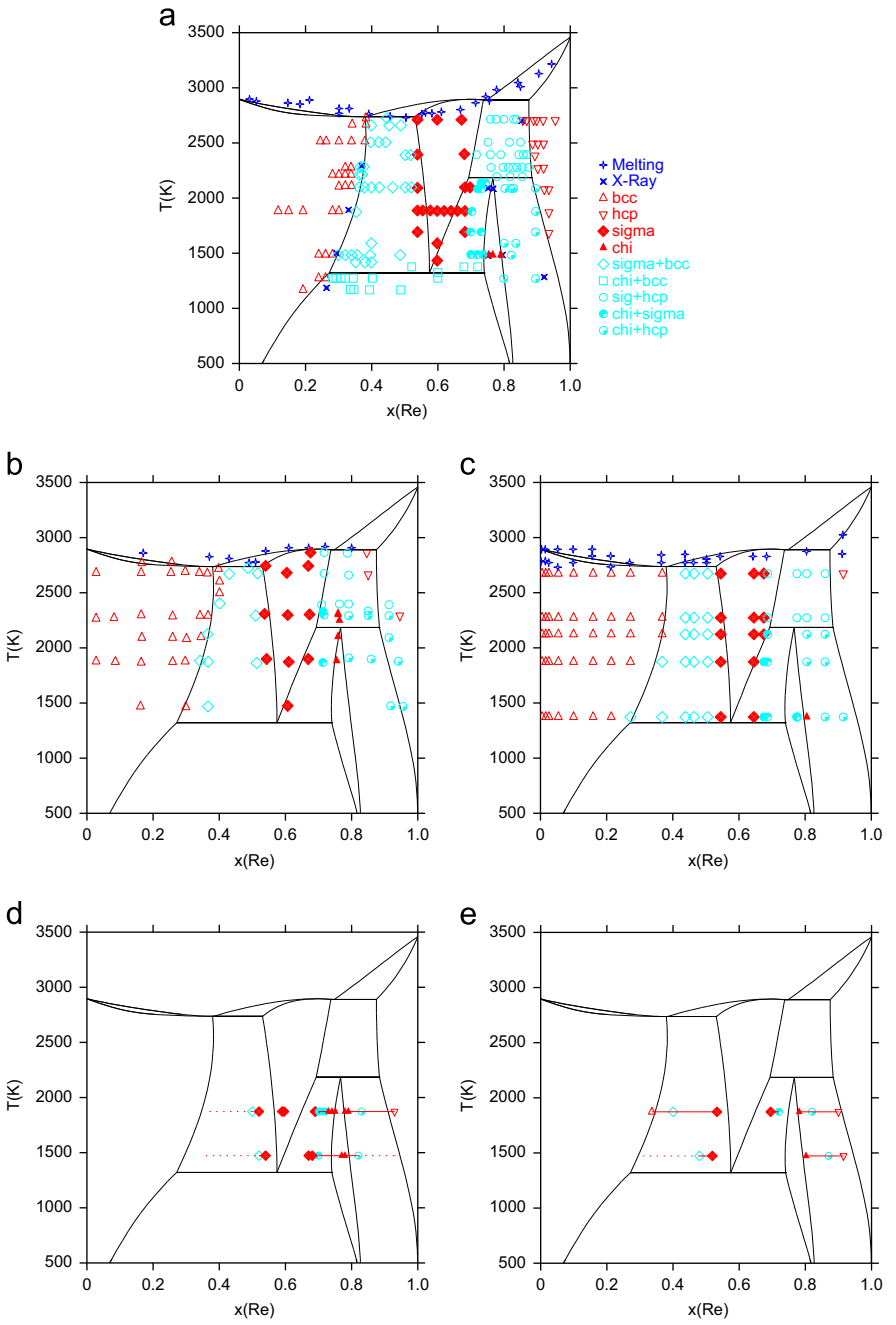


Fig. 5. Comparison between the calculated Mo–Re phase diagram from this work and experimental data from (a) Knapton [20], (b) Dickinson and Richardson [19], (c) Savitskii et al. [21,22], (d) Farzadfar et al. [25] and (e) Yaqoob and Joubert [32].

necessary to reach equilibrium may be prohibitive and experiments in this area should be considered cautiously. This is in particular true for casted alloys. The phases formed at high temperature having a coarse structure need very long time to reach equilibrium at low temperature. For the melting temperatures, their very high values induce experimental difficulties implying high uncertainties. As discussed in Section 2.1, the liquidus data by Dickinson and Richardson [19] are preferred in the present modeling. The calculated diagram shows good agreement with these data but Knapton liquidus measurements [20] also follow reasonably well the calculated melting, as well as the data from Savitskii [21,22]. The calculated phase diagram generally agrees with the experimental Re solubility in Mo and Mo solubility in Re. The agreement is better with the hcp solvus drawn by Knapton. The solubility of Mo in Re, extrapolated to room temperatures, is found to be very small.

The calculated invariant reactions are listed in Table 2 together with the experimental data from [19–22]. Excellent agreement is reached for the temperature 2890 K of the invariant reaction with the liquid, hcp and σ phases when compared to the experimental values of 2918 K from [19]. Nevertheless, the calculated transformation is eutectic, with formation of σ and hcp phases from the liquid while a peritectic reaction was proposed experimentally. As the σ and liquid compositions are very close (74 and 75 at.% Re), this difference is not significant. A close analysis of the microstructure shown in the different experimental papers has not allowed to clearly identify a peritectic morphology. The peritectic nature of this reaction seems to have been attributed only from

the evolution of the melting temperature. Considering the low accuracy of these, the nature of this reaction can be considered uncertain. It would be interesting to reinvestigate this point with the experimental facilities available nowadays. The eutectic reaction at 2713 K shows slightly less agreement. The larger discrepancy in Re content, notably for bcc and liquid, may be due to the large uncertainties in experimental data at these high temperatures. On the other hand the agreement is satisfactory for the temperature. Excellent agreement is also seen in the peritectoid at 78 at.% Re when compared to the experimental values of 76 at.% Re from [19], with a calculated temperature between experimental data from Dickinson and Richardson [19] and Savitskii et al. [21,22]. Finally, the present work calculates a eutectoid reaction at 27.1 at.% Re and a temperature of 1322 K in close agreement with the 29 at.% Re reported by Knapton [20] and close to the lower value of temperature (1373 K) proposed by [20].

The present phase diagram is also compared to those from previous descriptions [8,25,45–47], in Fig. 6 and in Table 2. Whatever the studies, the calculated phase boundaries in the solid-state globally agree with experimental observation from Dickinson and Richardson [19], Knapton [20], Savitskii et al. [21,22] works within the experimental uncertainties. The liquidus in the Re rich part is significantly higher for Mao et al. [8,45], Farzadfar et al. [25] and Yang et al. [46].

Some differences may be noted in the invariant temperatures (Table 2). The temperature of the peritectic is higher in Mao's work. It is 2966 K compared to 2918 K from Dickinson and Richardson [19] which is the highest temperature among the experimental determinations reasonably fitted by Farzadfar, Yang , Dupin and this work. The temperature of the eutectic is much higher in the different descriptions than in our calculation. But, our temperature is closer to the value determined by Knapton [20]. The peritectoid temperature, determined in this study, is intermediate among those from the others descriptions. Finally, temperature of the eutectoid is lower than the value determined by Knapton [20], whatever the descriptions.

Other differences may be noted in the description of the homogeneity domain of the σ and χ phases. While our description shows a rather V shape for the σ field when approaching the eutectoid reaction, the other descriptions, and in particular Mao's show a more rounded shape. This was obtained thanks to the use of excess parameters in order to try to fit the σ single phase alloys reported at the lower experimental temperature. However none of all these descriptions manage to agree with the wide σ homogeneity range at 1693 K reported by Knapton [20].

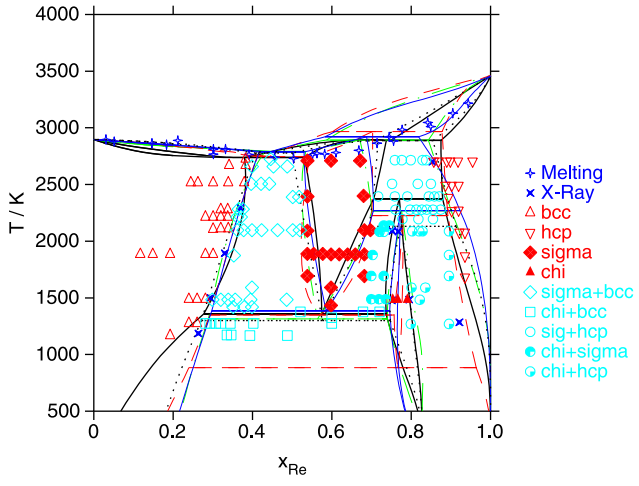


Fig. 6. Comparison between the calculated Mo–Re phase diagram (in black) with previous descriptions from Mao et al. ([8,45], dashed red), Farzadfar et al. ([25], green), Yang et al. ([46], blue), Dupin et al. ([47], black dotted line) and experimental data from Knapton [20]. (For interpretation of the references to color in this figure caption, the reader is referred to the web version of this paper.)

Results from Mao et al. and Yang et al. show that the composition range for χ phase is smaller than experimental data, and χ phase is not stable at low temperature with Mao's description. On the contrary, results from Farzadfar et al., Dupin et al. and this study show that the calculated composition range for χ phase is equivalent to the experimental data. The difference in composition ranges for χ phase between Farzadfar et al. and Yang et al. is surprising as these two studies use the same model for χ phase. Such difference could simply be explained by the subjectivity of any assessment, including CALPHAD type. This is one of the reasons why the increasing use of FP results should be promoted. They allow to decrease the subjectivity of the assessment.

Finally, differences appear for solubility in the terminal solutions. The differences on the Mo solubility in Re remain in the experimental uncertainty. The Re solubility in Mo calculated with the present work significantly differs from the previous descriptions at low temperature. This difference mostly comes from the use of SQS results for the solution phases. No experimental knowledge are available in this range in order to confirm that our description is better or not.

4.2. Simplifications of the σ phase modeling

The different simplifications introduced in Section 3.2.3 are first considered without excess parameters. Fig. 7a shows the calculated phase diagrams using all these simplifications without excess term. The phase diagram calculated with the 4SL simplification is identical to the 5SL full description one. However this is not a general conclusion. Among the different systems currently under consideration, the present authors studied some cases where some differences appear; this is generally the case if the energy of the configuration similar to ReMoMoMoMo or MoMoMoReMo would fall below the line between σ Mo and ReMoMoReMo. The 3SL-23 and 3SL-25 simplifications slightly underestimate the stability of σ phase. The liquidus temperatures are only slightly affected while the invariant eutectoid and peritectoid are significantly increased. The 2SL phase diagram is identical to the 3SL-35 one; the σ phase is not stable.

Fig. 8a shows the ordering enthalpies of the σ phase calculated with the different ideal simplifications. They are compared to the 5SL full description and to the DFT values. Open circles show the whole set of DFT results. Different colored symbols are used to identify the end-members used in the different simplifications (also see Table 4).

First of all, as expected from the phase diagram calculation, whatever the temperature considered, the 4SL simplification is identical to the full 5SL description. For the other cases, the differences can be commented in relation with the different configurations used and their DFT ordering energies. At low temperature, they are all identical to the 5SL in the 0–33 at.% Re composition range. This is due to the fact that all the models use the most stable configuration at 33 at.% Re: ReMoMoReMo. When raising the temperature this is not anymore true but the curves stay relatively close; more differences are observed at higher Re content where the σ phase is stable.

At low temperature, the 3SL-25 curve is very close to 5SL. It is actually below in the 33–60 at.% Re range. This is due to the fact that other configurations used in the 5SL at 60 at.% Re, and in particular the ReMoMoReRe, green cross, of energy very close to the most stable ReMoReReMo is not taken into account. At higher Re composition, this curve passes above the 5SL as the ReReReReMo and ReMoReReRe that are on the DFT convex hull are not used. At higher temperatures, the 3SL-25 ordering enthalpies are close to the 5SL but slightly above, in particular in the range of stability of the

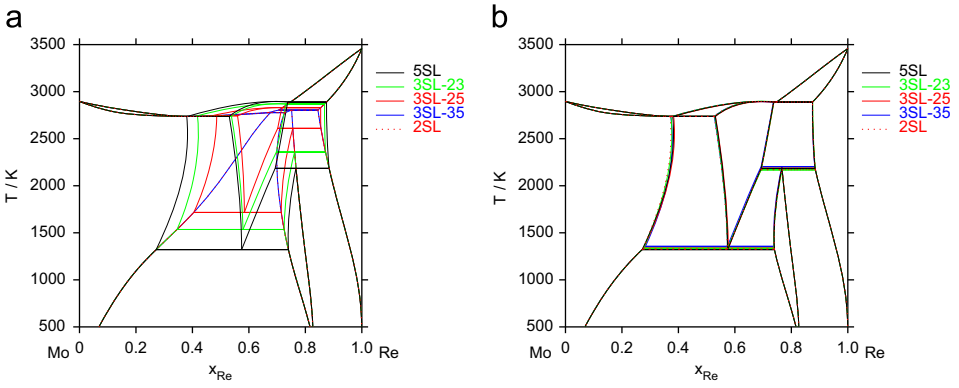


Fig. 7. The calculated Mo–Re phase diagram with the 5SL-CEF, shown in black, is compared to the different simplifications without excess terms (a) and with excess terms (b): 3SL-23 in green, 3SL-25 in red and 3SL-35 in blue. (For interpretation of the references to color in this figure caption, the reader is referred to the web version of this paper.)

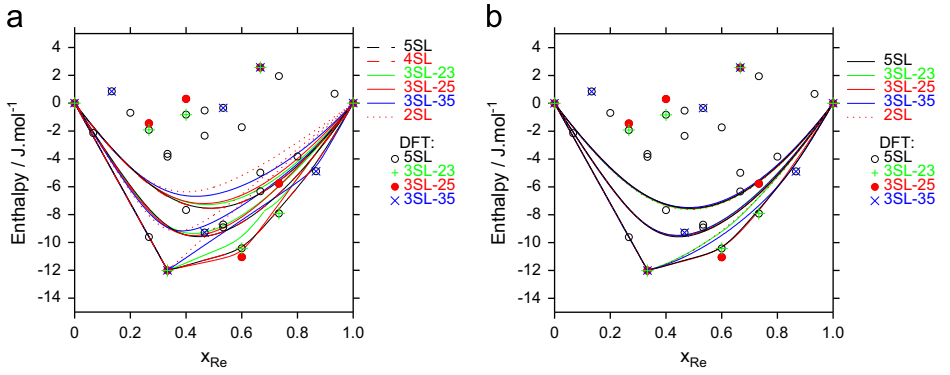


Fig. 8. Ordering enthalpies of the σ phase. The black open circles (○) correspond to the DFT values of all the 32 compounds listed in Table 4 referred to the values of the pure Re and Mo configurations. The enthalpies calculated at 500, 1500 and 2500 K with the 5SL-CEF, shown in black, are compared to the different simplifications without excess terms (a) and using the excess terms (b) listed in Table 8. The end-members used by 3SL simplifications are reported with the corresponding color. Reference states are σ-Mo and σ-Re at the current temperature. (For interpretation of the references to color in this figure caption, the reader is referred to the web version of this paper.)

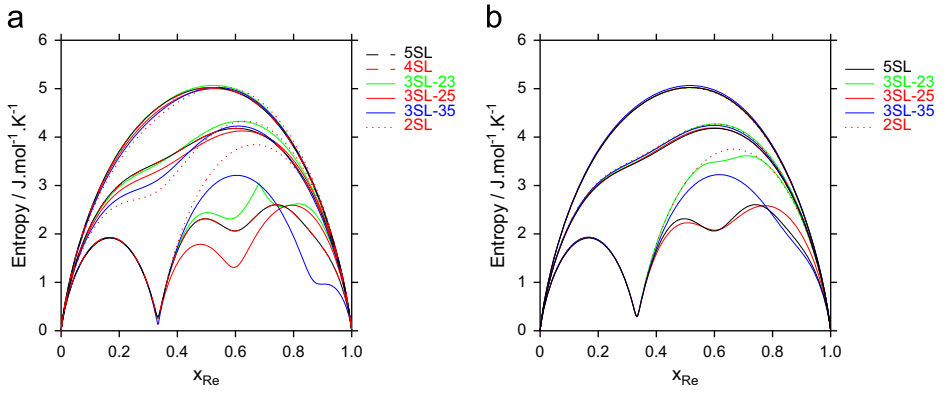


Fig. 9. The entropies of formation of the σ phase with the 5SL-CEF, shown in black, is compared to the different simplifications without excess terms (a) and with excess terms (b). The different sets of line are calculated at 500, 1500 and 2500 K. Reference states are σ-Mo and σ-Re at the current temperature. (For interpretation of the references to color in this figure caption, the reader is referred to the web version of this paper.)

phase, contributing to its lesser stability. This is due to the missing configurations mentioned in the discussion of the low temperature curve.

The 3SL-23 simplification corresponds to the same overall model $(A,B)_{10}(A,B)_{12}(A,B)_8$ than the 3SL-25 just discussed. They moreover use a very similar energy at 60 at.% Re. However their behavior at low temperature is significantly different as the 3SL-23 shows a miscibility gap around 67 at.% Re. This is due to the quite high stability of the configuration ReReReReMo at 73 at.% Re that falls below the line between ReMoMoReRe and the σ Re. The change of configuration between ReMoMoReRe and ReReReReMo implies too many sublattices to occur continuously at low temperature and thus yield a miscibility gap. At the higher temperatures considered the 3SL-23 curve is quite close to the 3SL-25. It actually passes below it at the higher temperature, *i.e.* closer to the 5SL full description, explaining that the corresponding phase diagram is closer to the 5SL. This is due to the stabilization induced by the configuration at 73 at.% Re.

The 3SL-35 simplification largely underestimates the ordering energy in the range of stability of the σ phase whatever the

temperature considered. This is mainly due to the fact that no end-compound at 60 at.% Re is used. The case of the 2SL simplification is quite similar.

Fig. 9a shows the σ configuration entropies calculated with the ideal simplifications at 500, 1500 and 2500 K compared to the full description. Once again the 4SL is identical to the 5SL even if very slight differences can be noticed on the Mo rich side at high temperatures. As for the enthalpy curves all the simplifications are identical to the 5SL in the 0–33 at.% Re composition range at 500 K. However when coming closer to Mo_2Re, slight differences are noticeable; the simplest models actually show slightly lower configurational entropy. The differences in the rest of the composition range are more important. Both 3SL-25 and 3SL-23, corresponding to the model $(A,B)_{10}(A,B)_{12}(A,B)_8$, show a minimum at the composition 60 at.% Re corresponding to the $Re_{10}Mo_{12}Re_8$ end-members, similar to the 5SL, while the 3SL-35 shows a minimum corresponding to the $Re_{10}Mo_4Re_{16}$ end-member and the 2SL none. The 3SL-25 that is the closer to 5SL in enthalpy at 500 K has a significantly lower entropy in the range of stability of the σ phase. That is explained by the fact that configuration of significant stability is missing. The 3SL-23 is actually closer in entropy to the 5SL than the 3SL-25 thanks to the important competition between the end-members at 60 and 73 at.% Re. The fact that the other compound of high stability at 60 at.% Re is missing actually induces an overestimation of the configurational entropy in the range of stability of the σ phase. This allows to obtain the phase diagram closer to 5SL. The 3SL-35 and 2SL also significantly overestimate the configurational entropy but their ordering enthalpies are too far from the 5SL full description to be compensated.

As discussed above, decreasing the number of sublattices implies that some of the interactions contributing to the stability of the phase are ignored. In order to compensate for these missing interactions, excess terms have to be introduced. For the different simplifications, a single excess parameter allows to get a phase diagram similar to the full 5SL description. The parameters assessed in order to obtain the present results are given in Table 8 for each description. The phase diagram calculated with the different models is shown Fig. 7b. They are very close. Slight differences are noticeable in the eutectoid and peritectoid temperatures and on the Re solubility in the bcc at high temperatures. Whatever the simplification considered, a single excess parameter allows to obtain a calculated phase diagram in agreement with the experimental information. The enthalpic part of this excess term is significantly bigger for the 3SL-35 and 2SL models that were largely underestimating the energies in their ideal approximation.

Fig. 8b shows the ordering enthalpy of the σ phase calculated at 500, 1500 and 2500 K with the different simplifications using assessed excess terms. The 3SL-25 is following the full 5SL description almost perfectly whatever the temperature. Surprisingly the negative interaction parameter induces a less negative ordering enthalpy; this can be explained by the fact that it increases the contribution of an end-member that is significantly less stable: ReReMoReRe, the red dot end-member at 73 at.% Re. The 3SL-23 ordering enthalpy is smoother than in the ideal case; the interaction parameter suppresses the miscibility gap. The difference with the full 5SL description is important at 500 K, very weak for the temperatures in the range of stability of the σ phase. The 3SL-35 and 2SL are coming closer to the full 5SL description whatever the temperature but remain significantly above in the σ stability composition range at 500 K. There is no way to follow the singular behavior at the 60 at.% Re composition without an end-member in the model for that.

Fig. 9b shows the configurational entropy of the σ phase calculated at 500, 1500 and 2500 K with the different simplifications using the assessed excess terms. They are compared to the full 5SL description. The 3SL-25 curve is significantly closer to the full 5SL description whatever the temperature considered. For the other simplifications, the 500 K curves stay rather far from the full 5SL description but come much closer for the higher temperatures. For the 3SL-23 simplification the curve at 500 K is smoother than in the ideal case but closer to the 2SL than to the 5SL.

In all the cases, the close phase diagram obtained thanks to the excess parameter indicates that the Gibbs energies are also very close in the temperature range where the σ phase is stable. The ordering enthalpy and configurational entropy are both very well approximated by the 4SL and 3SL-25 simplifications. However, the H/S separation is not accurately reproduced by the other simplifications. Describing σ phases that would be stable at low temperature with these models could be highly problematic, in particular if the assessor wants to keep physical basis for the different model parameters used.

The 3SL-25 model seems the most promising simplification. It corresponds to the general scheme $(A,B)_{10}(A,B)_{12}(A,B)_8$, *i.e.* $(A,B)_{10}{}^{4f+8j}(A,B)_{12}^{2a+8i_2}(A,B)_8^{8i_1}$. It is actually identical to the one from 3SL-23 even if the two descriptions are different from DFT results. It presents the advantage of having two important end-members $A_{10}B_{20}$ and $A_{18}B_{12}$ in the composition range where the σ phase is stabilized in most systems. This gives the opportunity to get a rather flat energy curve at low temperatures between these two compounds as observed in Mo–Re from DFT results.

5. Conclusion

A new Mo–Re thermodynamic description has been derived using first-principle calculations and experimental data. Ab initio results have been used in the framework of the compound energy formalism in order to describe the σ and χ phases with respectively 5 and 4SL considering both elements in all sublattices. The use of FP results allows to obtain a reasonable agreement with all the experimental information available with a limited number of assessed parameters.

Comparisons to descriptions previously derived for this system show the importance to introduce all the elements in all sublattices in order to properly describe the configurational entropy of the σ phase.

CEF simplifications for the σ phase are investigated, still using ab initio energy data of the end-members. Reasonable agreement with the experimental phase diagram has been possible thanks to the use of excess parameters in the different 3SL simplifications considered as well as for the 2SL simplification. While some of the models previously proposed seem unable to approximate closely the low temperature 5SL full description, the 4SL merging the 2*a* and $8i_2$ sites and a new 3SL merging the 4*f* and 8*j* sites, $(A,B)_{10}(A,B)_{12}(A,B)_8$, are more promising. This is to be confirmed in other systems, binary and ternary.

It is difficult to relate the important difference in the vibrational entropy of pure Mo in the σ phase between this work and the previous one [7] to the only fact that the SQS values are used for the solid solution phases. It would be of high interest to estimate the vibrational entropy of the σ phase for the pure elements by some FP approach.

Acknowledgments

Financial support from Agence Nationale de la Recherche (ANR) (Armide 2010 BLAN 912 01) is acknowledged. DFT calculations were performed using HPC resources from GENCI-CINES (Grant 2011-96175).

Appendix A. Supplementary material

Supplementary data associated with this article can be found in the online version at http://dx.doi.org/10.1016/j.calphad.2013.08.002.

References

[1] R.-C. Reed, The Superalloys Fundamentals and Applications, Cambridge University Press, New York, 2008, ISBN: 978-0511541285.
[2] C.M.F. Rae, R.C. Reed, Acta Mater. 49 (2001) 4413–4425.
[3] H.L. Lukas, S.G. Fries, B. Sundman, Computational Thermodynamics, Cambridge University Press, Cambridge, 2007, ISBN:978-0521868112.
[4] J.-C. Zhao, M.F. Henry, Adv. Eng. Mater. 4 (2002) 501–508.
[5] J.-O. Andersson, A. Fernandez Guillermet, M. Hillert, B. Jansson, B. Sundman, Acta Metall. 34 (1986) 437–445.
[6] J.-O. Andersson, B. Sundman, CALPHAD 11 (1987) 83–92.
[7] I. Ansara, T.G. Chart, A. Fernandez Guillermet, F.H. Hayes, U.R. Kattner, D.G. Pettifor, N. Saunders, K. Zeng, CALPHAD 21 (1997) 171–218.
[8] P. Mao, K. Han, Y. Xin, J. Alloys Compd. 299 (2008) 153–162.
[9] Z.K. Liu, Y. Chang, J. Alloys Compd. 464 (2008) 190–196.
[10] J.-M. Joubert, Prog. Mater. Sci. 53 (2008) 528–583.
[11] S.G. Fries, B. Sundman, Phys. Rev. B 66 (2002) 012203.
[12] N. Dupin, S.G. Fries, J.-M. Joubert, B. Sundman, M.H.F. Sluiter, Y. Kawazoe, A. Pasturel, Philos. Mag. 86 (2006) 1631–1641.
[13] M. Sluiter, A. Pasturel, Phys. Rev. B 80 (2012) 134122.
[14] J.-C. Crivello, J.-M. Joubert, J. Phys. Condens. Matter 22 (2010) 035402.
[15] M. Palumbo, T. Abe, C. Kocer, H. Murakami, H. Onodera, CALPHAD 34 (2010) 495–503.
[16] M. Palumbo, T. Abe, S.G. Fries, A. Pasturel, Phys. Rev. B 83 (2011) 144109.
[17] K. Yaqoob, J.-C. Crivello, J.-M. Joubert, Inorg. Chem. 51 (2012) 3071–3078.
[18] M. Palumbo, S.G. Fries, T. Hammerschmidt, T. Abe, J.-C. Crivello, A. Breidi, J.M. Joubert, R. Drautz, Comput. Mater. Sci. (2013), http://dx.doi.org/10.1016/j.commatsci.2013.08.051.
[19] J.M. Dickinson, L.S. Richardson, Trans. ASM 51 (1958) 1055–1071.
[20] A.G. Knapton, J. Inst. Met. 87 (1958–1959) 62–64.
[21] E.M. Savitskii, M.A. Tylkina, K.B. Povarova, Zh. Neorg. Khim. 4 (1959) 424–434.
[22] E.M. Savitskii, M.A. Tylkina, K.B. Povarova, Russ. J. Inorg. Chem. 4 (1959) 190–195.
[23] N.V. Ageev, V.S. Shekhtman, Bull. Acad. Sci. USSR, Phys. Ser. 23 (5) (1959) 638–639.
[24] C.G. Wilson, Acta Crystallogr. 16 (1963) 724–730.
[25] S.A. Farzadfar, M. Levesque, M. Phejar, J.M. Joubert, CALPHAD 33 (2009) 502–510.
[26] J.-M. Joubert, M. Phejar, Prog. Mater. Sci. 54 (2009) 945–980.
[27] J.R. Gavaler, M.A. Janocko, C.K. Jones, Appl. Phys. Lett. (1972) 179–180.
[28] E. Valderrama, C. James, M. Krishnan, X. Zhao, K. Seo, F.A. Stevie, P. Maheshwari, in: Proceedings of SRF2011, Chicago, IL, USA.
[29] L. Brewer, R.H. Lamoreaux, Atom. Energ. Rev., Spec. Issue 7 (1980) 195–356.
[30] K.J. Leonard, J.T. Busby, S.J. Zinkle, J. Nucl. Mater. 366 (2007) 369–387.
[31] H. Bei, Y. Yang, G.B. Viswanathan, C.J. Rawn, E.P. George, J. Tiley, Y.A. Chang, Acta Mater. 58 (2010) 6027–6034.
[32] K. Yaqoob, J.M. Joubert, J. Alloys Compd. 559 (2013) 101–111.
[33] A. Breidi, J.C. Crivello, J.M. Joubert, in preparation.
[34] A. Zunger, S.-H. Wei, L.G. Ferreira, J.E. Bernard, Phys. Rev. Lett. 65 (1990) 353–356.
[35] G. Ghosh, A. van de Walle, M. Asta, Acta Mater. 56 (2008) 3202–3221.
[36] C. Jiang, C. Wolverton, J. Sofo, L.Q. Chen, Z.K. Liu, Phys. Rev. B 69 (2004) 214202.
[37] D. Shin, R. Arroyave, Z.K. Liu, A. Van de Walle, Phys. Rev. B 74 (2006) 024204.
[38] SGTE Unary database, version 4.4, ⟨http://www.sgte.org⟩ (accessed 20.7.2001).
[39] A. Dinsdale, CALPHAD 15 (1991) 317–425.
[40] Y. Wang, S. Curtarolo, C. Jiang, R. Arroyave, T. Wang, G. Ceder, L.-Q. Chen, Z.-K. Liu, CALPHAD 28 (2004) 79–90.
[41] A.E. Kissavos, S. Shallcross, V. Meded, L. Kaufman, I.A. Abrikosov, CALPHAD 29 (2005) 17–23.
[42] J.-C. Crivello, A. Breidi, J.M. Joubert, Inorg. Chem. 52 (2013) 3674–3686.
[43] P. Hohenberg, W. Kohn, Phys. Rev. B 136 (1964) 864–871.
[44] W. Kohn, L.J. Sham, Phys. Rev. A 140 (1965) 1133–1140.
[45] P. Mao, K. Han, Y. Xin, J. Alloys Compd. 482 (2009) 557–558.
[46] Y. Yang, C. Zhang, S. Chen, D. Morgan, Y.A. Chang, Intermetallics 18 (2010) 574–581.
[47] N. Dupin, J.-C. Crivello, A. Breidi, J.-M. Joubert, K. Yaqoob, J.-M. Fiorani, in: CALPHAD XLI (2012) abs:Wm3; ⟨http://nathdupin.free.fr/public/Lectures/monire.pdf⟩.
[48] O. Redlich, A.T. Kister, J. Ind. Eng. Chem. 40 (1948) 341–345.
[49] B. Sundman, J. Agren, J. Phys. Chem. Solids 42 (1981) 297–301.
[50] B. Jansson, PhD Thesis, Division of Physical Metallurgy, Stockholm, Sweden, Royal Institute of Technology, 1984.
[51] B. Sundman, B. Jansson, J.-O. Andersson, CALPHAD 9 (1985) 153–190.